Biosensors and Bioelectronics 220 (2023) 114857

Contents lists available at ScienceDirect

Biosensors and Bioelectronics

journal homepage: www.elsevier.com/locate/bios

# Smartphone-based immunochemical sensor exploiting peroxidase-like activity of ligand-capped gold nanostars: A proof-of-concept detection of *Mycobacterium bovis*

Javier Lou-Franco [a], Yunfeng Zhao [a,b], Joost L.D. Nelis [a,c], Linda Stewart [a], Karen Rafferty [b], Christopher Elliott [a,d], Cuong Cao [a,e,*]

[a] Institute for Global Food Security, School of Biological Sciences, Queen's University of Belfast, 19 Chlorine Gardens, Belfast, BT9 5DL, UK
[b] School of Electronics, Electrical Engineering and Computer Science, Queen's University Belfast, Stranmillis Road, Belfast, UK
[c] CSIRO Agriculture and Food, 306 Carmody Rd, St Lucia QLD, 4067, Australia
[d] School of Food Science and Technology, Faculty of Science and Technology, Thammasat University, 99 Mhu 18, Pahonyothin Road, Khong Luang, Pathum Thani 12120, Thailand
[e] Material and Advanced Technologies for Healthcare, Queen's University of Belfast, 18-30 Malone Road, Belfast, BT9 5BN, UK

ARTICLE INFO

*Keywords:*
Gold nanostar
Peroxidase-mimicking
Mycobacterium bovis
Biosensor
Smartphone
Food pathogen

ABSTRACT

Bacterial pathogens represent a safety concern in the food industry, and this is amplified by the lack of sensing devices that can be applied on-site by non-trained personnel. In this study, peroxidase-mimicking activity of gold nanostars was exploited to develop a user-friendly colourimetric sensor. A smartphone was exploited as an image reader and analyser, empowered with a novel App developed in-house. The mobile App was evaluated and compared with a commercial smartphone App for its capability to quantify generated colourimetric signals. A major obstacle found with sensors relying on gold nanozymes is the fact that modification of the surface of gold nanoparticles with biorecognition elements generally lead to a suppression of their nanozyme activity. This drawback was overcome by introducing an autocatalytic growth step, which successfully restored the peroxidase-mimicking activity through generation of new gold nanoseeds acting as catalytic centres. A proof-of-concept using this sensing mechanism was developed targeting *Mycobacterium bovis*, a zoonotic pathogen primarily found in cattle but that can be transmitted to humans by consumption of contaminated food and cause tuberculosis disease. The resulting smartphone-based immunological sensor has shown promising results with a linear response between $10^4$ – $10^6$ CFU/mL, enabling detection of *M. bovis* at concentrations as low as $7.2{\cdot}10^3$ CFU/mL in buffer conditions. It is anticipated that the concept of the developed approach will have applicability in many fields relying on smartphone-based biosensing.

## 1. Introduction

Gold nanoparticles (AuNP) are among the most promising tools in the field of biosensing due to the many physicochemical properties derived from the nanoscale, which include enhanced spectroscopic signals (Logan et al., 2021; Pawar et al., 2019) and enzyme-mimicking properties (Das et al., 2021; Lou-Franco et al., 2021). These features are modulated by the morphology of AuNP (Kelly et al., 2003), with anisotropic NP displaying interesting advantages such as the "lightning-rod effect" or a larger surface area. The former relates to the high confinement of the electromagnetic energy present at the sharp edges or tips of anisotropic NP, also known as hot spots and making these materials excellent surface-enhanced Raman scattering (SERS) substrates (Indrasekara et al., 2014; Murphy et al., 2005). The larger surface area, on the other hand, lies behind their increased chemical reactivity and explains the enhanced catalytic properties reported for anisotropic NP (Lou-Franco et al., 2021; Sajanlal et al., 2011). Gold nanostars (AuNSt) have recently gained much attention due to the presence of multiple sharp branches that provide them both with a large number of hot spots and a high surface-area-to-volume ratio. Many studies have proven the suitability of AuNSt as SERS substrates. However, not much information has been collected on whether their nanozyme behaviour can be improved compared to spherical NP or their biological counterparts.

* Corresponding author. Institute for Global Food Security, School of Biological Sciences, Queen's University of Belfast, 19 Chlorine Gardens, Belfast, BT9 5DL, UK.
*E-mail address:* c.cao@qub.ac.uk (C. Cao).

https://doi.org/10.1016/j.bios.2022.114857
Received 17 August 2022; Received in revised form 6 October 2022; Accepted 23 October 2022
Available online 31 October 2022

Smartphones, on the other hand, have become an important ally for portable data processing and user-friendly analysis thanks to their rapid development and accessibility: nowadays almost 4 billion smartphones are used all over the world. These phones are equipped with a camera that may serve as a low-cost tool for on-site colourimetric analyses. Despite the potential of combining gold nanozymes and smartphones for biosensing, only two studies are reported in the scientific literature exploiting this combination in any configuration (Han et al., 2017; Hsu et al., 2020). This can be explained by AuNP exhibiting suppressed catalytic properties when their surface is modified, which generally is an essential step for developing biosensing devices. In this study, the peroxidase-like activity of surface-modified AuNSt was evaluated and characterised, and an autocatalytic growth step (Cao et al., 2011) introduced to compensate for suppression of peroxidase-like activity which has previously prevented progression of this methodology. A proof-of-concept assay was developed using antibodies previously produced for detection of *Mycobacterium bovis* (Stewart et al., 2012).

*Mycobacterium bovis* belongs to the *Mycobacterium tuberculosis* complex (MTBC), a group of mycobacteria that cause tuberculosis disease (TB) in both humans and animals. *Mycobacterium tuberculosis* is the main causative organism of TB in humans and represents one of the main causes of death worldwide (Lozano et al., 2012). The World Health Organization (WHO) estimated that there were 1.2 million TB deaths in 2018 (WHO, 2019). Other members of the MTBC which can cause TB in humans include *M. bovis* which is host-adapted to cattle and causes bovine tuberculosis (bTB), a significant animal health issue in many countries. When *M. bovis* is transmitted to humans it can cause zoonotic TB (zTB), and it can also cause TB in other animal species including wildlife (Aranaz et al., 2004; Delahay et al., 2002; Matos et al., 2016). *M. bovis* is estimated to account for 10–15% of TB cases in developing countries and 1–2% in developed countries (Bolaños et al., 2017). These estimates are thought to be imprecise as most cases of human TB are assumed to be caused by *M. tuberculosis* as *M. bovis* and *M. tuberculosis* are >99.95% similar at the genomic level (Garnier et al., 2003) and indistinguishable clinically and morphologically (Torres-Gonzalez et al., 2016). Recent literature has indicated that regions previously declared bTB-free for more than 10 years are reporting a rise in the number of human infections with a zoonotic origin (Lombardi et al., 2017). This represents an important barrier for controlling the global TB epidemic and hinders many efforts to eradicate the disease. The main route of transmission of *M. bovis* to humans is through consumption of contaminated dairy products. There is therefore a necessity to test foodstuff, especially dairy products which are consumed raw, for the presence of *M. bovis* before it reaches the consumer. To date, however, no point-of-care sensing devices exist to target *M. bovis* and meet the food sector needs, which include on-site testing by non-trained personnel (Nelis et al., 2019b). Current methodologies for detecting *M. bovis* are mostly based on culture methods. These combine microbial isolation with phenotypic and biochemical characterisation, but are time consuming as it can take up to 90 days to identify slow-growing species like *M. bovis* (Bolaños et al., 2017; de Azevedo Issa et al., 2017; Thoen et al., 2014). Other approaches such as PCR (Adams et al., 2013) require trained personnel and sophisticated laboratory equipment; and rapid assays, such as Xpert® MTB/RIF, are unable to differentiate between the various *Mycobacterium tuberculosis* complex species, compounding the underdiagnosis of zTB. Electrochemical (Chena et al., 2015; Lermo et al., 2010) and optoelectronic (Silva et al., 2011) biosensors have been developed for *M. bovis* detection, although they have not yet achieved the level of standardisation required for use in routine analyses. Therefore, food samples at risk of being contaminated with *M. bovis* are not specifically tested.

The proof-of-concept smartphone-based competitive immunological approach developed in this work for specific detection of *M. bovis* exploits the peroxidase-like activity of ligand-capped gold nanostars and identified a solution to the common problem of suppressed catalytic activity after functionalisation of AuNP with biorecognition elements. The reported approach could pave the way for development of point-of-care sensors for potential use in a wide range of areas beyond food safety, including biomedicine or environmental analyses.

## 2. Materials and methods

### 2.1. Chemicals and reagents

Gold(III) chloride trihydrate ($HAuCl_4{\cdot}3H_2O$, 99.9%), L-ascorbic acid ($C_6H_8O_6$), silver nitrate ($AgNO_3$), hydrochloric acid (HCl), sodium citrate tribasic dehydrate ($HOC(COONa)(CH_2COONa)_2{\cdot}2H_2O$, 99%), 11-mercaptoundecanoic acid ($HS(CH_2)_{10}CO_2H$, 95%), O-(3-Carboxypropyl)-O′-[2-(3-mercaptopropionylamino)ethyl]-polyethylene glycol (Mw 5000), O-(2-Carboxyethyl)-O′-(2-mercaptoethyl)heptaethylene glycol ($C_{19}H_{38}O_{10}S$, 95%), 3,3′,5,5′-tetramethybenzidine (TMB), hydrogen peroxide ($H_2O_2$ 30% (w/w) in $H_2O$), dithiothreitol (DTT), phosphate buffer saline (PBS, pH 7.4) were all purchased from Sigma Aldrich (UK). TEM Formvar carbon films on nickel grids were purchased from Agar Scientific (UK). *Mycobacterium bovis*, *Mycobacterium smegmatis*, *Escherichia coli* K12, *Escherichia coli* BL21 and α-*M. bovis* antibodies were sourced locally at the School of Biological Sciences, Queen's University Belfast. *M. bovis* suspensions were subjected to a 10 kGy dose of gamma radiation (Gammabeam 650 cobalt irradiator, AFBI, Belfast) prior to use and then cultured on Middlebrook 7H10 agar for 56 days to ensure complete inactivation of the bacteria.

### 2.2. Analysis instrumentation

Ultraviolet–Visible spectroscopic analyses were conducted using an Agilent Technologies Cary 60 UV–Vis spectrophotometer. Microtiter plate absorbance measurements were performed using a Safire$^2$ TECAN microplate reader. Gold nanoparticles dynamic light scattering (DLS) and ζ-sizer measurements were carried out using a Zetasizer NanoZS (Malvern). Transmission electron microscopy (TEM) imaging was conducted on a Joel JEM 1400 Plus Transmission Electron Microscope, operated at 120 kV, while high resolution transmission electron microscopy (HR-TEM) imaging was conducted on a TALOS FEI HR-TEM operated at 200 kV (ThermoFisher). Images captured with a Samsung Galaxy S10 were analysed using *Colour detector* App (currently *RGB Colour Detector*) produced by The Programmer and freely accessible from PlayStore, and an in-house developed App (Section 2.7).

### 2.3. Synthesis of gold nanostars (AuNSt)

AuNSt were synthesised using a seed-mediated approach, following Liz-Marzán protocol with minor modifications (Logan et al., 2021; Serrano-Montes et al., 2016). Briefly, a seed solution of gold nanospheres was prepared by adding 5 mL of 1% sodium citrate solution to 95 mL of boiling 0.5 mM $HAuCl_4$ solution while stirring vigorously. After 15 min, the solution was cooled and kept at 4 °C. The produced seeds exhibited a Localised Surface Plasmon Resonance (LSPR) of 519 nm. Varying volumes (40–300 μL) of these citrate-stabilised seeds were added to 10 mL of 0.25 mM $HAuCl_4$ containing 10 μL of 1 M HCl in a glass vial while stirring moderately. 100 μL of 3 mM $AgNO_3$ and 50 μL of 100 mM L-AA were added immediately and the resulting solution allowed to react at room temperature (RT) for 2 min. A colour change is quickly observed, turning from light red to blue/greenish.

Once synthesised, the AuNSt were stabilised using one of the following coating molecules: sodium citrate (NaCit), 11-mercaptoundecanoic acid (11-MUA), α-mercapto-ω-carboxy-polyethylene glycol (PEG) or α-mercapto-ω-carboxy-oligoethylene glycol (OEG). In the first case, AuNSt were incubated overnight (O/N) in 1 M sodium citrate (final concentration), at RT and under mild stirring conditions. In the case of 11-MUA, citrate molecules were replaced with 11-MUA at a concentration of 100 μM in an ethanol:water 1:1 solution (v/v), O/N at RT and under mild stirring conditions. Alternatively, the AuNSt were also

stabilised with hydrophilic polymers (PEG or OEG). Immediately after synthesis, 0.8 μM of PEG was added to the AuNSt solution and stirred continuously for 15 min at RT. Stabilisation with OEG was achieved by adding 500 μM of OEG to the AuNSt solution and stirred O/N at RT. Regardless of the stabilisation method used, the AuNSt were finally centrifuged at 10 °C and 1200 RCF for 25 min to remove any unbound molecule and resuspended in $dH_2O$.

### 2.4. Catalytic studies of AuNSt as peroxidase-mimics

100 pM of AuNSt was incubated with varying concentrations of TMB (0–0.5 mM) in 300 μL of 6% $H_2O_2$ aqueous solution for 20 min at RT. The absorbance of each reaction was measured at a wavelength of 370 nm, which is representative of the charge transfer complex derived from the TMB oxidation (Laing et al., 2011; McVey et al., 2019). These absorbance values were converted into concentration of oxTMB using the Beer-Lambert equation and plotted following the Hills model to extract the Michaelis-Menten parameters enabling comparison of the catalytic efficiency of the different AuNSt samples.

### 2.5. Functionalisation of AuNSt

The dithiothreitol (DTT) reduction method was used to prepare IgG antibodies containing sulfhydryl groups, with minor modifications from previously reported protocols (Ji et al., 2010). In short, a 200 μL solution of IgG antibody (QUBMA-Bov) produced previously (Das et al., 2022; Stewart et al., 2012) was prepared at a concentration of 1 mg/mL in PBS 0.1 M – EDTA 2 mM buffer. 8 μL of DTT 0.5 M prepared in aqueous solution was then added and the mixture incubated under gentle stirring for 25 min at RT. The reduced IgG antibody was immediately centrifuged 4 times using an Amicon Ultra-0.5 Centrifugal Filter (50 KDa) at 14000 RCF for 10 min, and resuspended in PBS – EDTA buffer to remove the excess of DTT thus limiting cleavage of disulphide bridges between the heavy and light chains of the antibody and maintaining their functional binding sites (Pathak et al., 2007). The reduced antibody was collected by spinning the container upside-down at 100 RCF for 2 min, and then added to a freshly prepared solution of bare AuNSt together with PEG at a final concentration of 10 μM. Subsequently, the mixture was left to react under gentle stirring for 30 min at RT. Finally, the functionalised AuNSt were centrifugated at 10 °C and 1200 RCF for 25 min to remove any unbound residues.

### 2.6. Competitive immunochemical assay for M. bovis detection

A $10^5$ CFU/mL dilution of the *M. bovis* was immobilised onto a microplate (Nunc-ImmunoTM 96 MicroWell™ MaxiSorp™) in 100 μL of coating buffer (carbonate/bicarbonate 0.1 M, pH 9.6). The plate was incubated O/N at 4 °C and the following day washed 4 times with wash buffer (PBS 10 mM/Tween 0.05%). Simultaneously, different concentrations of *M. bovis* ($10^3$–$10^6$ CFU/mL in PBS) were incubated with the functionalised AuNSt-QUBMA-Bov in wash buffer for 30 min, under gentle stirring at RT. The resulting AuNSt-QUBMA-Bov-*M. bovis* were then added to the microplate (100 μL per well) and incubated for 30 min under gentle stirring at RT. After washing the plate 4 times with wash buffer, 150 μL of growth solution ($2{\cdot}10^{-4}$ M $HAuCl_4$, $10^{-6}$ M L-AA and $10^{-6}$ M CTAB in $10^{-2}$ M phosphate buffer pH 7.4) was added to each well and incubated at RT for 45 min undisturbed. Finally, 150 μL of TMB (0.2 mg/mL) was added to each well and the absorption measured at 370 nm after 20 min (Scheme 1).

### 2.7. Smartphone app development

A smartphone App was developed to perform the solution-based colourimetry and interpret the assay results. The App automates the testing result interpretation and is capable of multiplexing (i.e., interpreting multiple samples at one time). It mainly consists of data generation, image pre-processing, and result predicting phases. In the data generation phase, another smartphone with a white screen was placed underneath the microplate to illuminate the coloured solutions from beneath and avoid reflection issues in the image, following previous

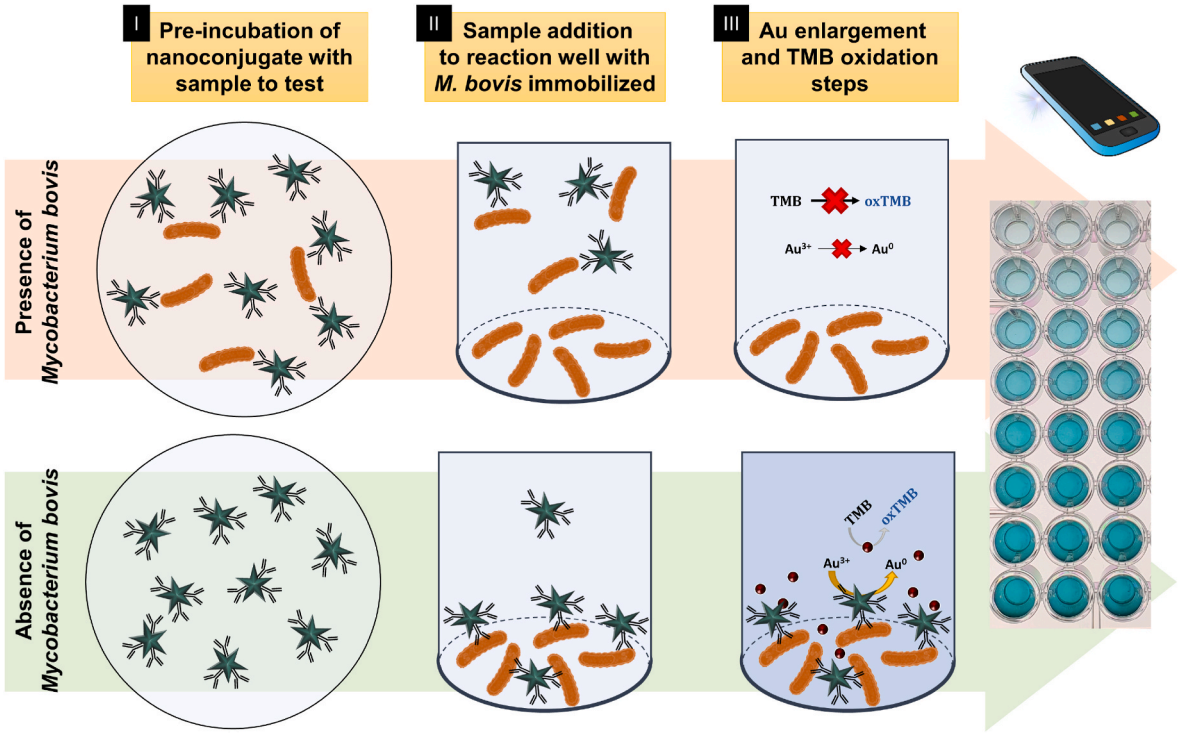


**Scheme 1. Proposed model for the detection of *M. bovis*.** The system is based on a competitive immunochemical assay using a secondary gold growth on captured AuNSt to restore the peroxidase-like activity, oxidising TMB into a blue product. A picture of the results is then taken with a smartphone for interpretation.

observations (Nelis et al., 2019a). The smartphone running the developed App was used to take images of the illuminated solution through its rear camera from above the microplate (Lee et al., 2019). In the second phase, the testing images are background subtracted using the algorithm proposed in (Zhao et al., 2018): $R_T = R_B \mathscr{F}^{-1}(D_T) / \mathscr{F}^{-1}(D_B)$, where $R_T$ and $R_B$ are the colour corrected testing and background image respectively, $D_T$ and $D_B$ are the original images taken by camera, and $\mathscr{F}^{-1}$ is the inverse camera response function. The processed LUV colour feature of each solution sample is collected using manually placed label markers in the smartphone App. Finally, the testing result is interpreted using the polynomial model: $h_\theta(l,u,v) = (\sum_{i=0}^{4} \sum_{j=0}^{4-i} \sum_{k=0}^{4-i-j} \theta_{ijk} l^i u^j v^k)^{10}$, where l, $u$, $v$ are the three colour channels of the LUV colour feature and $\theta$ is the feature vector (Zhao et al., 2019).

React Native (Eisenman, 2015) was used to construct the smartphone App for data generation and user interfaces, while Flask (Grinberg, 2018) was used to develop the cloud service for image pre-processing and result interpretation. Tensorflow (Abadi et al., 2016) was used as the machine learning framework and Adam Optimiser (Kingma and Ba, 2015) was used to perform the global optimisation and calculate the optimal feature vector.

## 3. Results and discussion

### 3.1. Synthesis and characterisation of AuNSt

AuNSt were produced with different optical and surface properties, which were then analysed for their potential to be used as nanozymes capable of generating a colourimetric signal. Prior to any surface modification, different AuNSt were produced following a seed-mediated approach described in Section 2.3 with minor modifications. The decrease in the amount of seeds used during the synthesis led to a larger final particle size (Khoury and Vo-Dinh, 2008) if the rest of the parameters were kept unchanged. This resulted in a LSPR shift to longer wavelengths with the consequential colour change in the AuNSt solutions (Fig. 1A). Thus, a smaller gold deposition onto the seeds led to more spherical-like nanostructures with LSPR around 600 nm and a dark blue colour, whilst a larger gold deposition was observed for syntheses with few seeds resulting in a larger LSPR shift, AuNSt with longer and sharper tips, and a greenish solution colour (Fig. S1). A representative sample of AuNSt was analysed by TEM (Fig. 1B). It was prepared using 50 μL of seeds, which resulted in a LSPR of 752 nm. Two hundred and six individual AuNSt from TEM results of the same sample were measured using ImageJ software. The average particle size (measured from tip to tip) was 105 ± 29 nm. This translates into a highly polydisperse sample, which can be observed in Fig. 1B as morphological differences between NP. DLS analysis of the same sample demonstrated an average particle diameter of 98 nm with a polydispersity index of 0.195. Generally, DLS measurements result in larger diameter values, since this approach considers the hydrodynamic particle diameter as opposed to TEM-based measurements. However, DLS calculations are based on a mathematical model fit for the Brownian motion of spherical particles in a solution, leading to less precise diameter values when star-shaped particles are analysed.

### 3.2. Peroxidase-like activity of AuNSt

A detailed kinetic analysis was performed prior to the utilisation of AuNSt in a colourimetric assay to detect *M. bovis*. As it has been previously reported, AuNPs exhibit a strong peroxidase-like activity amongst other enzymatic activities (Lou-Franco et al., 2021). This has been extensively studied for gold nanospheres elsewhere (McVey et al., 2019), but an in depth kinetic analysis of peroxidase-like activity of AuNSt is lacking. Considering that modifying the surface of AuNSt remains a necessary step for developing a functioning and specific biosensor, it is essential to understand how modifications affect the

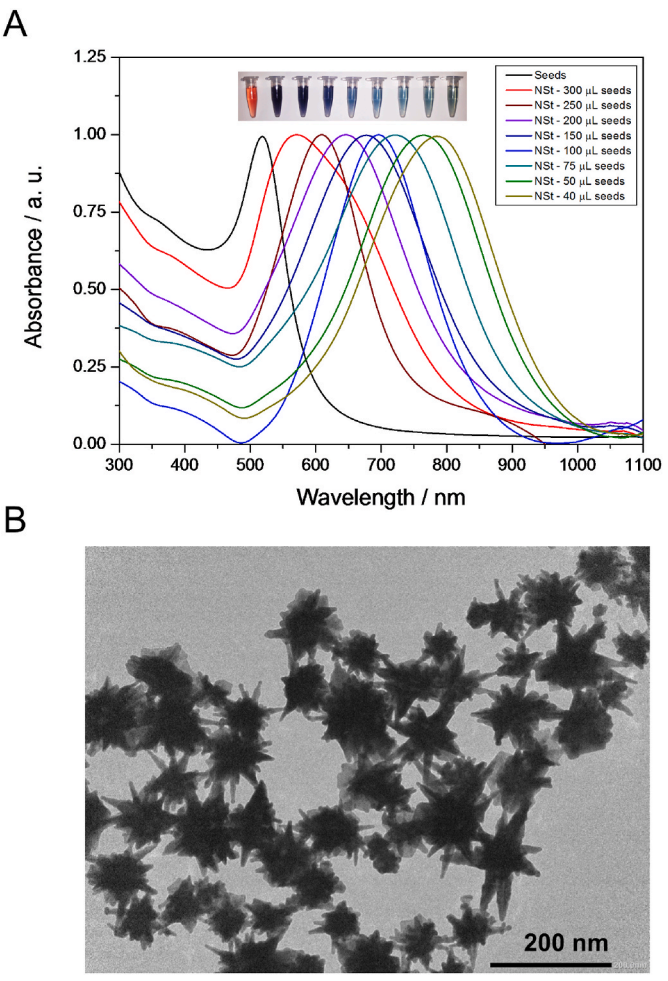


**Fig. 1.** Characterisation of AuNSt. (A) UV–Vis analyses of AuNSt-NaCit synthesised using various amounts of Au seeds (ranging from 40 to 300 μL) which resulted in different optical properties (picture inset). (B) TEM image of AuNSt-NaCit with LSPR at 752 nm. TEM operated at 120 kV and ×60000 magnification.

properties on which the sensing mechanism is based. Therefore, a solution containing 100 pM AuNSt synthesised with different LSPR responses (thus different sizes) was added to different concentrations of TMB ranging from 0 to 0.5 mM in the presence of 6% $H_2O_2$ (Fig. 2A). The oxidation of TMB into its radical cation ($TMB^+$) was observed after 20 min of reaction by measuring the absorbance of the solution at 370 nm (Laing et al., 2011). Although oxTMB is generally measured using $A_{650\ nm}$ or $A_{450\ nm}$, it was observed that the strong absorbance exhibited by AuNSt in the range 600–800 nm interferes with the $A_{650\ nm}$ value coming from oxTMB, whereas the acidic conditions required for developing $A_{450\ nm}$ were not compatible with AuNSt stability. Therefore, the $A_{370\ nm}$ value was used to initially calculate the concentration of oxTMB generated using the Beer-Lambert law and then the reaction rate as reported by McVey and co-workers (McVey et al., 2019). The resulting data was plotted and fitted using the Hill equation, which enabled determination of several kinetic parameters (Table S1). Comparing the data obtained from the three AuNSt sets with different LSPR values, it is observed that AuNSt with LSPR located at longer wavelengths led to a greater maximum rate of reaction and therefore to a larger turnover number ($k_{cat}$) (Fig. 2B). These observations are in agreement with previous studies, where nanostructures with higher surface area-to-volume ratio see their catalytic properties enhanced (Ma et al., 2017). As described in Section 3.1, greater LSPR values were observed for AuNSt with a larger gold deposition during the synthesis, which provides the

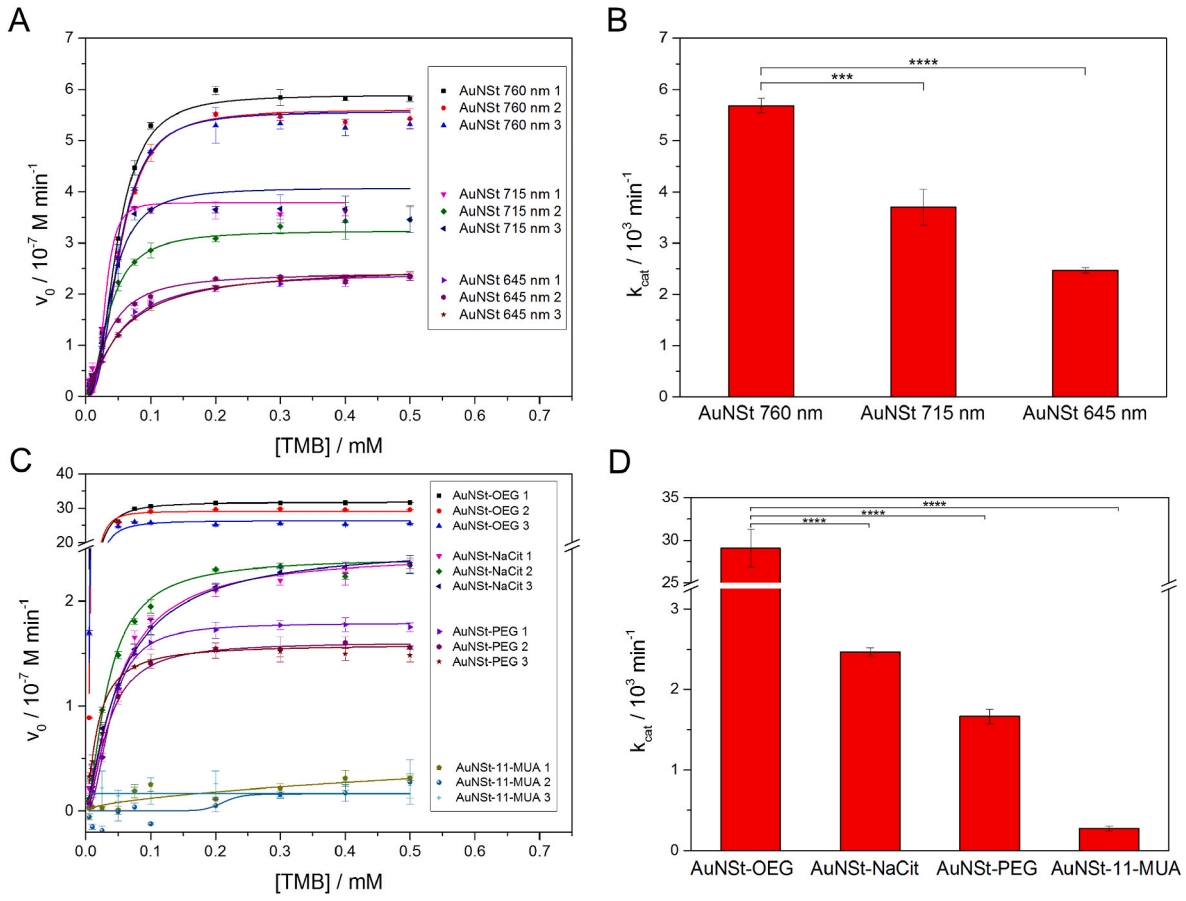


**Fig. 2.** Characterisation of the peroxidase-like activity of AuNSt exhibiting different plasmonic responses and surface modifications. (A) Kinetic analysis of AuNSt-NaCit displaying different LSPR modes in the presence of varying concentrations of TMB (0–0.5 mM) and 6% $H_2O_2$. (B) Comparison of the turnover number ($k_{cat}$) observed for AuNSt-NaCit with different LSPR modes. (C) Kinetic analysis of AuNSt coated with different stabilizing molecules in the presence of varying concentrations of TMB (0–0.5 mM) and 6% $H_2O_2$. (D) Comparison of the turnover number observed for AuNSt coated with different stabilizing molecules. Data in (A) and (C) are fitted to a Hill equation while a one-way ANOVA was performed to analyse data in (B) and (D).

AuNSt with sharper and longer tips and therefore a larger gold surface area to act as a catalyst centre. However, AuNSt analysed so far are electrostatically stabilised with NaCit, which means that any further functionalisation of the NPs surface using the carboxylic groups present in the citrate molecules will not be covalently attached to the NP surface and therefore risk being released from its surface. Thus, the versatility of the AuNSt surface chemistry was used to immobilise various stabilizing molecules (-PEG, -OEG, −11-MUA) taking advantage of the gold-sulphur interaction that leads to strong bonds. A ζ-potential analysis was conducted to characterise the stability and surface properties of these AuNSt (Fig. S2). Subsequently, they were used in a similar kinetic analysis (Fig. 2C) where different degrees of surface hindrance were observed. Comparison of the turnover numbers for each AuNSt indicated that surface coating played an important role in the observed peroxidase-like activity (Fig. 2D), and depends on the chemical nature and 3-dimensional organization of the self-assembled monolayers (SAMs) onto the gold surface (Love et al., 2005). As such, 11-MUA was expected to form a highly dense SAM exposing the carboxylic groups to the outside, due to the hydrophobic interactions between the aliphatic chains. This would impede the substrate (TMB) from reaching the gold surface, thus explaining the virtual non-existent peroxidase-like activity observed. In the case of AuNSt-PEG, the hydrophilicity of the chains should avoid the formation of highly dense SAMs, leading to increased catalytic rates because of a better surface accessibility by the substrate. Similarly, hydrophilic moieties in AuNSt-NaCit do not represent a significant surface hindrance, displaying an increased peroxidase-like activity as compared to 11-MUA- and PEG-coated AuNSt, due to the ease with which these electrostatically attached molecules can be replaced by substrate molecules. However, AuNSt-OEG showed a surprising 10-fold increase in peroxidase-like activity when compared to AuNSt-PEG. A hypothesis can be proposed to explain this phenomenon based on the literature. Firstly, studies have shown that long polymeric chains are arranged following the dumbbell model (Pai et al., 2011), resulting in a random coil adjacent to the gold surface which would reduce the substrate adsorption rate. However, the smaller length of OEG SAMs could result in a helical conformation where two consecutive O atoms of the OEG chain would orientate with an angle of 90°, generating an electrostatic field enhancement in the regions next to them and forming strong hydrogen bond structures with surrounding H atoms from water molecules (Wang et al., 1997). Consequently, helical OEG layers strongly absorb water, serving as a template for water nucleation and enabling a faster diffusion of TMB molecules towards the gold surface, which may explain the observed higher catalytic rate.

### 3.3. *Autocatalytic growth and peroxidase-like activity of protein coated AuNSt*

Surface modification of AuNSt with biorecognition elements is an essential step during the development of diagnostic assays. Nevertheless, previous studies have shown that functionalisation typically comes at the cost to the catalytic properties of AuNSt (Lou et al., 2018). To overcome this, an autocatalytic growth step was proposed to restore the peroxidase-like activity of protein coated AuNSt. This was based on a secondary gold growth, previously reported elsewhere

(Rodríguez-Lorenzo et al., 2012), *via* the surface reduction of $HAuCl_4$ to $Au^0$ in the presence of a weak reducing agent (L-AA) and using cetyltrimethylammonium bromide (CTAB) as a stabiliser (Fig. 3A). Under these conditions, AuNSt act as catalysts for the spontaneous growth of particles by decreasing the threshold energy of the reaction, a step that has been well documented (Johnson et al., 2002). The HR-TEM analysis showed that, after performing the autocatalytic growth step, not only was AuNSt growth observed leading to less spiky NPs, but also nanocrystal formation occurred, forming new seeds which detached from the AuNSt surface (Fig. 3B). This is in agreement with previous observations using gold nanospheres (Cao et al., 2011; Zayats et al., 2005). These gold seeds display an easily accessible bare surface that can act as a catalytic centre and oxidise TMB molecules. To prove that the autocatalytic growth could effectively restore the peroxidase-like activity, AuNSt-PEG ($A_{750\ nm} = 1$) was functionalised with 100 μg/mL streptavidin and incubated with 10 μM EDC for 2 h with minor stirring. Both PEG and streptavidin were chosen as model linker and protein, respectively, to study and to optimise the growth step. Two sets of 100 pM AuNSt-streptavidin were enlarged using a growth solution ($2{\cdot}10^{-4}$ M $HAuCl_4$, $10^{-6}$ M L-AA and $10^{-6}$ CTAB in $10^{-2}$ M phosphate buffer pH 7.4) while a third set of AuNSt-streptavidin was not enlarged. After 20 min of reaction, TMB was added to each solution to a final concentration of 0.1 mM and its oxidation into oxTMB followed during the first 10 min of reaction by measuring the $A_{370nm}$. The results showed that only the samples containing AuNSt-streptavidin that had undergone a secondary gold growth had restored catalytic properties and turned blue, while the sample where no gold growth was performed remained inactive (Fig. 3C). Moreover, as a negative control, the gold growth reaction was performed on a sample without the presence of AuNSt to confirm that the formation of gold seeds did not occur, discarding false positive signals in the absence of AuNSt.

### 3.4. Sensitivity and selectivity

Prior to the smartphone analysis, the assay was first optimised and characterised using a spectrophotometer. This enabled determination of the sensitivity of the assay and demonstrated the selectivity towards *M. bovis*. Different concentrations of *M. bovis* were tested ranging from $10^3$ to $10^6$ CFU/mL. The oxidation of TMB was followed by measuring the $A_{370nm}$ with a spectrophotometer after 20 min reaction time. The results showed a decreasing signal proportional to the increase in the concentration of *M. bovis* (Fig. 4A). These data were plotted and fitted ($R^2 = 0.998$) to a dose-response curve, showing a limit of detection (LOD) of $7.2{\cdot}10^3$ CFU/mL, calculated as 3 times the standard deviation of the negative sample. A linear trend is observed in the range $10^4$–$10^6$ CFU/mL, although due to cell culture limitations, larger bacterial concentrations were not available to reach a plateau effect to determine the saturation point of the assay. The results observed resembled those

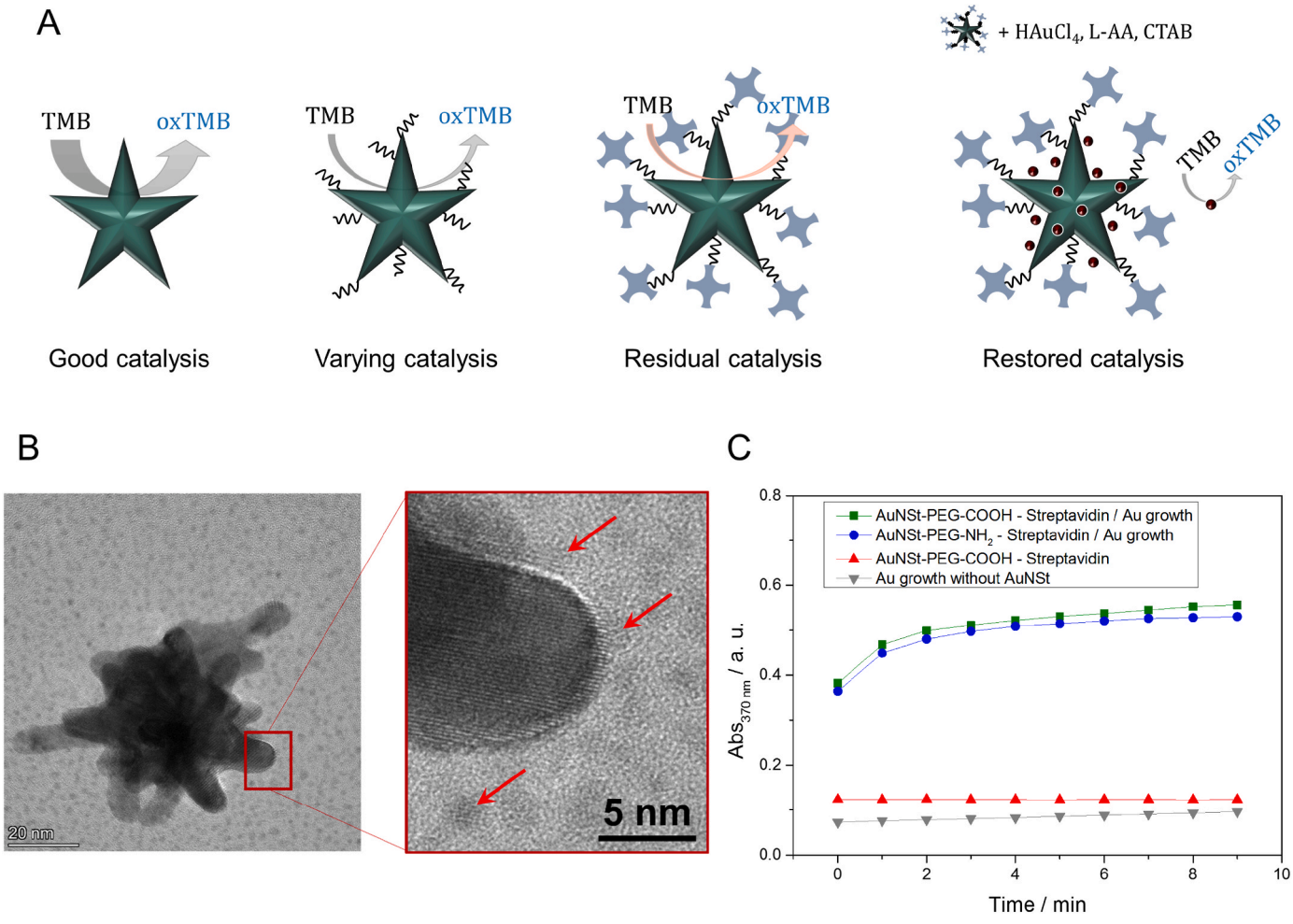


**Fig. 3.** Autocatalytic growth assay to restore the catalytic activity of protein-coated AuNSt. (A) Proposed model based on observations for peroxidase-like activity of AuNSt coated with different molecules. Bare, polymer- and protein-coated AuNSt display varying catalytic properties which are restored applying an autocatalytic growth step. (B) HR-TEM image of AuNSt after performing an autocatalytic growth, where 100 pM of AuNSt-streptavidin reacted with $2{\cdot}10^{-4}$ M $HAuCl_4$, $10^{-6}$ M L-AA and $10^{-6}$ CTAB in $10^{-2}$ M phosphate buffer pH 7.4. Red arrows point to newly formed nanoseeds, acting as catalytic centres. (C) UV–Vis analysis of restored peroxidase-like activity of AuNSt coated with streptavidin with and without autocatalytic growth.

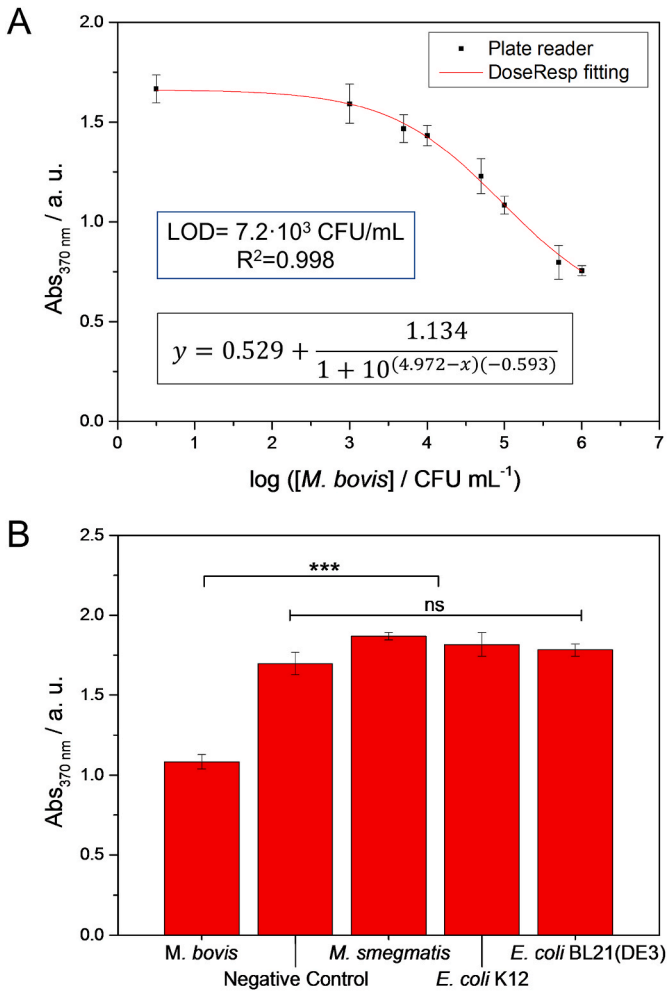


**Fig. 4.** Sensitivity and selectivity analyses of the proposed system to detect *M. bovis*. (A) Calibration curve of the assay. *M. bovis* samples ranging from $10^3$ to $10^6$ CFU/mL were tested and the $A_{370}$ values measured plotted and fitted to a dose-response curve. The LOD was calculated as 3 times the standard deviation of the negative control. (B) Selectivity assay where different bacteria at a same concentration ($10^5$ CFU/mL) were analysed and the results compared through a one-way ANOVA (n = 3).

described previously in the literature (Chena et al., 2015; Stewart et al., 2017). Chena and co-workers developed an amperometric immunosensor capable of detecting *M. bovis* in milk samples with a detection limit of $3.5{\cdot}10^3$ CFU/mL and a linear range from $10^4$ to $10^6$ CFU/mL (Chena et al., 2015). This attempt to simplify the detection of *M. bovis* was performed using a *Mycobacterium tuberculosis* specific antibody, which was also able to bind *M. bovis*, thus resulting in a rapid and effective biosensor lacking selectivity within the MTB complex. Stewart and co-workers developed a novel lateral flow device (LFD) aimed at detecting *M. bovis* in badger faeces (Stewart et al., 2017), as badgers are well known for being important carriers of *M. bovis*. The LFD approach was combined with an immunomagnetic separation (IMS) step to concentrate *M. bovis* cells prior to detection. Their assay also showed positive results for samples containing high numbers of *M. bovis* cells ($\geq 10^{4-5}$ CFU/g) in line with the sensitivity values reported herein. More recently, ferromagnetic AuNP (Gilbride et al., 2021) and biogenic AuNP (Das et al., 2022) have been used to develop colourimetric assays, improving the LOD values reported above. These systems, however, still rely on expensive lab-based readout equipment, while at the same time cannot escape the limited robustness of immunoassays for detecting small bacterial concentrations.

Regarding the selectivity of the assay, several bacteria were tested to prove that the signal differences observed in the sensitivity assay were due to an effective IgG-bacteria binding event and not to an unspecific attachment of the AuNSt to the bacteria surface. Three different bacteria and a negative control were analysed and compared to *M. bovis*, including *Escherichia coli* K12, *Escherichia coli* BL21(DE3) and *Mycobacterium smegmatis*. Each of the bacterial cultures were tested at $10^5$ CFU/mL and the $A_{370nm}$ measured with a spectrophotometer (Fig. 4B). A one-way ANOVA comparing the signal observed in the negative control and the 3 non-specific samples was not-significant, whereas the comparison of all these assays with the *M.-bovis* assay was significant (p-value $< 0.001$). Therefore, the assay can be considered specific for *M. bovis*, while reaching a sensitivity similar to that observed in other studies.

### 3.5. Smartphone-based detection

Once the sensitivity and specificity of the assay were determined, two smartphone Apps were used as readout systems to predict *M. bovis* concentrations from the colourimetric signal generated in the assay. One of them was freely available in PlayStore ("RGB Colour Detector", formerly "Colour detector"), and the other one was an in-house App developed as described in Section 2.7 ("QuantColorimetryApp"). In both cases an image taken with a smartphone was imported and analysed. *Colour detector* is a system that enables detection and measurement of colour signals using multiple colour spaces: RGB, CMYK, HSV, HTML, HEX, HSL or RAL. From these, RGB was used for this assay, as recent comprehensive analyses confirmed that it is a robust space for colour analyses in sensing devices and is rarely outperformed by other models (Nelis et al., 2019a, 2020). Further analyses were conducted to determine the optimum colour channel to quantify the appearance of the blue colour generated by the TMB oxidation process (Fig. 5). Different concentrations of AuNSt ranging from 50 to 400 pM were used as catalysts after undergoing a secondary gold growth as described in Section 2.6 to

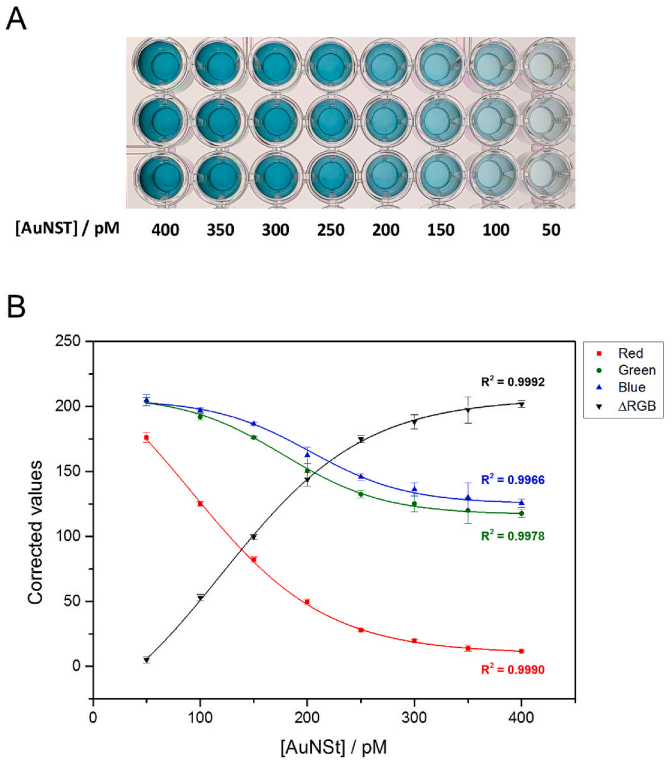


**Fig. 5.** Colour analysis of TMB oxidation process generated by the presence of different concentrations of AuNSt (ranging from 50 to 400 pM) subjected to a secondary gold growth. Data were (A) captured with a smartphone (Samsung Galaxy S10) and (B) analysed using the *Colour detector* App.

ensure their optimum peroxidase-like activity. TMB (0.3 mM) was added to each sample and an image taken after 20 min of reaction (Fig. 5A). The image was uploaded to the *Colour detector* App and the RGB values for each well extracted to process and analyse the data. Each well was analysed in 3 different spots of the well to ensure the image colour was homogeneous all over the well and at the same time, each AuNSt concentration was analysed in triplicate. The resulting values were averaged and corrected using the background signal (i.e. that generated by analysing the colour of an empty well). This was calculated as follows:

$$Corrected\ value = \frac{Original\ value^2}{Background\ signal}$$

This correction was applied to the R, G and B values obtained from the App, while a different approach was used for calculating ΔRGB, using the next equation:

$$\Delta RGB = \sqrt{(R_i - R_0)^2 + (G_i - G_0)^2 + (B_i - B_0)^2}$$

Both the red channel (R) and a mathematical combination of the three channels (ΔRGB) showed good results for oxTMB colourimetric quantification (Fig. 5B). However, the R channel measurements showed a greater robustness towards errors than ΔRGB, thus the R channel values were chosen for quantifying the assay's results. Next, the *Colour detector* App was calibrated using images from the *M. bovis* assay, by associating each bacterial concentration to a specific R value, so every new measurement can be interpolated to an unknown bacterial concentration through a Dose-Response equation fitting.

To prove the applicability of the proposed assay, several *M. bovis* samples prepared in buffer were analysed and the blue colour generated was quantified using the *Colour detector* App after taking a picture of the results (Fig. 6A) (quantification was performed using the red channel as discussed in Fig. 5, see Fig. S3 for more information of the process). The smartphone analysis showed a good prediction with a slope close to 1 ($R^2 = 0.978$) when the actual *M. bovis* concentration is plotted against the predicted *M. bovis* concentration using the *Colour detector* App. A similar study was undertaken using an in-house developed App as the readout system to quantify the colour signal generated in the assay (Fig. S4). As previously the App was calibrated prior to any prediction, however, the *QuantColorimetryApp* uses a polynomial regression fitting curve to predict unknown values in new measurements instead of providing a result in any of the colour spaces above discussed. The predictions obtained using the *QuantColorimetryApp* did show a trend but a slope of 1.46 ($R^2 = 0.839$) and larger error bars indicated that further optimisation was still required to achieve an accurate quantitative readout system. All smartphone results were compared with the predictions made using the spectrophotometer (Fig. 6B), where a slope of 0.99 and a coefficient of determination of 0.99 manifested the accuracy of the lab-based readout systems. The mean absolute error (MAE) of each readout system was determined and compared, and showed that the spectrophotometer had a MAE of 4.5 ± 2.4%, the *Colour detector* App 6.4 ± 1.5%, and the *QuantColorimetryApp* 15.4 ± 5.9%. The larger MAE of the latter can be attributed to an imperfect polynomial regression curve used by the App for the predictions, whose imprecise fitting would translate into larger error bars. This would not be the case for the *Colour detector* App, where a calibration curve following a Dose-Response equation showed a much better fitting and, therefore, an equally better accuracy in the predictions. From these data, it can be concluded that smartphone-based readout systems are catching up in terms of the accuracy reached by lab-based technologies, while providing portability and accessibility to the end-user.

## 4. Conclusions

A competitive immunochemical assay based on the nanozyme activity of gold nanostars has been devised for the development of a proof-of-concept food-borne bacterial pathogen detection. The peroxidase-like

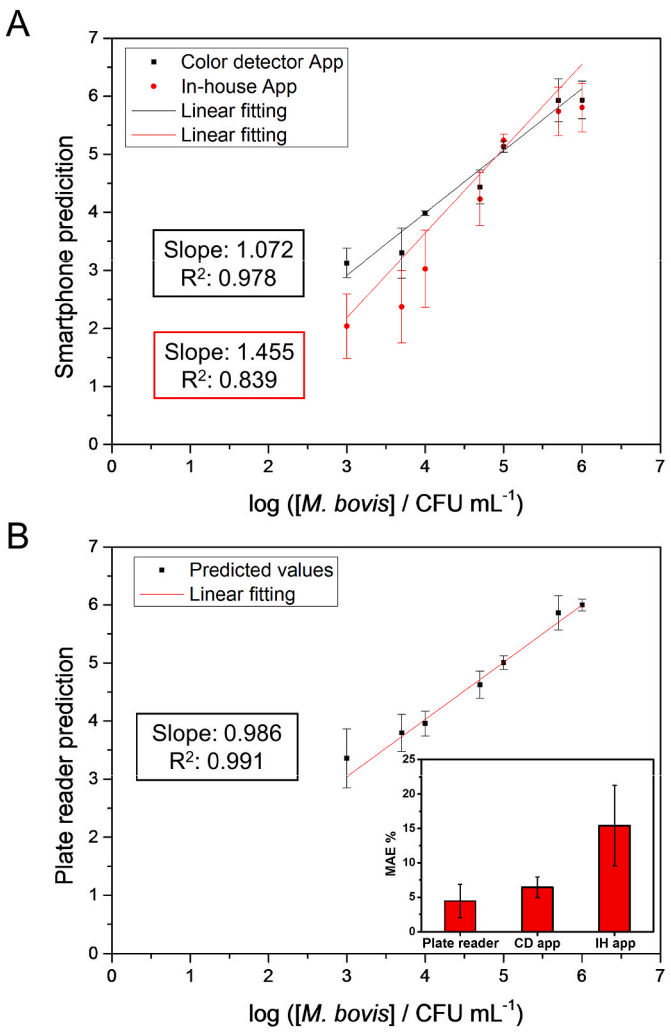


**Fig. 6.** Smartphone-based detection of *M. bovis*. (A) Two different smartphone Apps were used to analyse the images. After calibration, both Apps were capable of predicting the concentration of *M. bovis* present in several samples ranging from $10^3$ to $10^6$ CFU/mL. (B) Predictions observed using the spectrophotometer and comparison of the accuracy in the predictions with both smartphone Apps.

activity of AuNSt was extensively characterised to provide an insight of the underlying mechanism and apply it in a real sensor device. Using *M. bovis* as a target in the assay, it was observed that QUBMA-Bov-coated AuNSt lost their capability to act as peroxidase mimics. Therefore, a secondary gold growth, generating more centres for catalysis, was required to restore the nanozyme activity. The developed approach showed a sensitivity of $7.2 \cdot 10^3$ CFU/mL in buffer conditions without any enrichment step. Moreover, the assay takes less than 3 h to perform and exhibits a minimal cross-reactivity with the inter- and intra-genus bacteria evaluated. Several smartphone-based readout systems were successfully used to determine the presence of the bacteria, including two smartphone Apps whose performance was compared to that of a lab-based spectrophotometer. The accuracy of the smartphone Apps predictions indicate a step forward towards portability and accessibility of food testing, replacing expensive lab-based readout systems with user-friendly smartphone Apps. Commercial Apps exist displaying a better accuracy for colour quantification than the App herein developed, but they still require data processing steps that need to be performed by the user. On the other hand, the App developed in this study can be calibrated in advance for any specific assay, directly providing a prediction result in the desired units, which adds an important benefit that is not

found in commonly commercialised smartphone Apps. With their strengths and current weaknesses, the fields of biosensing and software development will likely work together for many years.

## CRediT authorship contribution statement

**Javier Lou-Franco:** Conceptualization, Methodology, Data curation, Investigation, Writing – original draft, Writing – review & editing. **Yunfeng Zhao:** Writing – review & editing. **Joost L.D. Nelis:** Methodology, Data curation, Writing – review & editing. **Linda Stewart:** Resources, Methodology, Writing – review & editing. **Karen Rafferty:** App development. **Christopher Elliott:** Conceptualization, Funding acquisition, Project administration, Supervision, Writing – review & editing. **Cuong Cao:** Conceptualization, Data curation, Funding acquisition, Project administration, Supervision, Writing – original draft, Writing – review & editing.

## Declaration of competing interest

The authors declare that they have no known competing financial interests or personal relationships that could have appeared to influence the work reported in this paper.

## Data availability

Data will be made available on request.

## Acknowledgements

The authors J.L., Y.Z., J.L.D.N., K.R., C.E. and C.C. acknowledge funding from the European Union's Horizon 2020 research and innovation program under the Marie Sklodowska-Curie Grant Agreement No. 720325. J.L. also wishes to acknowledge the support provided by J. Pablo Salvador and M. Pilar Marco in the field of immunochemistry.

## Appendix A. Supplementary data

Supplementary data to this article can be found online at https://doi.org/10.1016/j.bios.2022.114857.

## References

Abadi, M., Agarwal, A., Barham, P., Brevdo, E., Chen, Z., Citro, C., Corrado, G.S., Davis, A., Dean, J., Devin, M., Ghemawat, S., Goodfellow, I., Harp, A., Irving, G., Isard, M., Jia, Y., Jozefowicz, R., Kaiser, L., Kudlur, M., Levenberg, J., Mane, D., Monga, R., Moore, S., Murray, D., Olah, C., Schuster, M., Shlens, J., Steiner, B., Sutskever, I., Talwar, K., Tucker, P., Vanhoucke, V., Vasudevan, V., Viegas, F., Vinyals, O., Warden, P., Wattenberg, M., Wicke, M., Yu, Y., Zheng, X., 2016. TensorFlow: large-scale machine learning on heterogeneous distributed systems. arXiv Prepr. arXiv1603.04467 1–19. https://doi.org/10.48550/arXiv.1603.04467.

Adams, A.P., Bolin, S.R., Fine, A.E., Bolin, C.A., Kaneene, J.B., 2013. Comparison of PCR versus culture for detection of Mycobacterium bovis after experimental inoculation of various matrices held under environmental conditions for extended periods. Appl. Environ. Microbiol. 79, 6501–6506. https://doi.org/10.1128/AEM.02032-13.

Aranaz, A., de Juan, L., Montero, N., Sanchez, C., Galka, M., Delso, C., Alvarez, J., Romero, B., Bezos, J., Vela, A.I., Briones, V., Mateos, A., Dominguez, L., 2004. Bovine tuberculosis (Mycobacterium bovis) in wildlife in Spain. J. Clin. Microbiol. 42, 2602–2608. https://doi.org/10.1128/JCM.42.6.2602.

Bolaños, C.A.D., de Paula, C.L., Guerra, S.T., Franco, M.M.J., Ribeiro, M.G., 2017. Diagnosis of mycobacteria in bovine milk: an overview. Rev. Inst. Med. Trop. Sao Paulo 59, 1–13. https://doi.org/10.1590/S1678-9946201759040.

Cao, C., Gontard, L.C., Thuy Tram, L.L., Wolff, A., Bang, D.D., 2011. Dual enlargement of gold nanoparticles: from mechanism to scanometric detection of pathogenic bacteria. Small 7, 1701–1708. https://doi.org/10.1002/smll.201100294.

Chena, Z., Wanga, W., Lib, H., Lib, Y., Chena, J., 2015. Rapid detection of Mycobacterium bovis in milk by a nanobiosensor. Int. J. Appl. Res. Vet. Med. 13, 93–99.

Das, B., Lou-Franco, J., Gilbride, B., Ellis, M.G., Stewart, L.D., Grant, I.R., Balasubramanian, P., Cao, C., 2022. Peroxidase-mimicking activity of biogenic gold nanoparticles produced from prunus nepalensis fruit extract : characterizations and application for the detection of Mycobacterium bovis. ACS Appl. Bio Mater. 5, 2712–2725. https://doi.org/10.1021/acsabm.2c00180.

Das, B., Lou-Franco, J., Logan, N., Balasubramanian, P., 2021. Nanozymes in point-of-care diagnosis: an emerging futuristic approach for biosensing. Nano-Micro Lett. 13, 1–51. https://doi.org/10.1007/s40820-021-00717-0.

de Azevedo Issa, M., Martins Soares Filho, P., Fonseca Júnior, A.A., Arrais Hodon, M., Cristian dos Santos, L., Karlisson Pimenta dos Reis, J., Cerqueira Leite, R., 2017. Comparative study of Mycobacterium bovis primary isolation methods. Braz. J. Microbiol. 48, 139–144. https://doi.org/10.1016/j.bjm.2016.07.026.

Delahay, R.J., De Leeuw, A.N.S., Barlow, A.M., Clifton-Hadley, R.S., Cheeseman, C.L., 2002. The status of Mycobacterium bovis infection in UK wild mammals: a review. Vet. J. 164, 90–105. https://doi.org/10.1053/tvjl.2001.0667.

Eisenman, B., 2015. Learning React Native: Building Native Mobile Apps with Javascript. O'Reilly Media, Inc.

Garnier, T., Eiglmeier, K., Camus, J.C., Medina, N., Mansoor, H., Pryor, M., Duthoy, S., Grondin, S., Lacroix, C., Monsempe, C., Simon, S., Harris, B., Atkin, R., Doggett, J., Mayes, R., Keating, L., Wheeler, P.R., Parkhill, J., Barrell, B.G., Cole, S.T., Gordon, S. V., Hewinson, R.G., 2003. The complete genome sequence of Mycobacterium bovis. Proc. Natl. Acad. Sci. U.S.A. 100, 7877–7882. https://doi.org/10.1073/pnas.1130426100.

Gilbride, B., Schmidt Garcia Moreira, G.M., Hust, M., Cao, C., Stewart, L., 2021. Catalytic ferromagnetic gold nanoparticle immunoassay for the detection and differentiation of Mycobacterium tuberculosis and Mycobacterium bovis. Anal. Chim. Acta 1184, 339037. https://doi.org/10.1016/j.aca.2021.339037.

Grinberg, M., 2018. Flask Web Development: Developing Web Applications with python. O'Reilly Media, Inc.

Han, K.N., Choi, J.S., Kwon, J., 2017. Gold nanozyme-based paper chip for colorimetric detection of mercury ions. Sci. Rep. 7, 1–7. https://doi.org/10.1038/s41598-017-02948-x.

Hsu, Y.P., Li, N.S., Chen, Y.T., Pang, H.H., Wei, K.C., Yang, H.W., 2020. A serological point-of-care test for Zika virus detection and infection surveillance using an enzyme-free vial immunosensor with a smartphone. Biosens. Bioelectron. 151, 1–9. https://doi.org/10.1016/j.bios.2019.111960.

Indrasekara, A.S.D.S., Meyers, S., Shubeita, S., Feldman, L.C., Gustafsson, T., Fabris, L., 2014. Gold nanostar substrates for SERS-based chemical sensing in the femtomolar regime. Nanoscale 6, 8891–8899. https://doi.org/10.1039/c4nr02513j.

Ji, T., Muenker, M.C., Papineni, R.V.L., Harder, J.W., Vizard, D.L., Mclaughlin, W.E., 2010. Increased sensitivity in antigen detection with fluorescent latex nanosphere-IgG antibody conjugates. Bioconjugate Chem. 21, 427–435. https://doi.org/10.1021/bc900295v.

Johnson, C.J., Dujardin, E., Davis, S.A., Murphy, C.J., Mann, S., 2002. Growth and form of gold nanorods prepared by seed-mediated, surfactant-directed synthesis. J. Mater. Chem. 12, 1765–1770. https://doi.org/10.1039/B200953F.

Kelly, K.L., Coronado, E., Zhao, L.L., Schatz, G.C., 2003. The optical properties of metal nanoparticles: the influence of size, shape, and dielectric environment. J. Phys. Chem. B 107, 668–677. https://doi.org/10.1021/jp026731y.

Khoury, C.G., Vo-Dinh, T., 2008. Gold nanostars for surface-enhanced Raman scattering: synthesis, characterization and optimization. J. Phys. Chem. C. Nanomater. Interfaces 112, 18849–18859.

Kingma, D.P., Ba, J., 2015. Adam: a method for stochastic optimization. arXiv Prepr 1–15. https://doi.org/10.48550/arXiv.1412.6980 arXiv1412.6980 ICLR 2015.

Laing, S., Hernandez-Santana, A., Sassmannshausen, J., Asquith, D.L., McInnes, I.B., Faulds, K., Graham, D., 2011. Quantitative detection of human tumor necrosis factor α by a resonance Raman enzyme-linked immunosorbent assay. Anal. Chem. 83, 297–302. https://doi.org/10.1021/ac1024039.

Lee, S., Thio, S.K., Park, S.Y., Bae, S., 2019. An automated 3D-printed smartphone platform integrated with optoelectrowetting (OEW) microfluidic chip for on-site monitoring of viable algae in water. Harmful Algae 88, 101638. https://doi.org/10.1016/j.hal.2019.101638.

Lermo, A., Liébana, S., Campoy, S., Fabiano, S., Inés García, M., Soutullo, A., Zumárraga, M.J., Alegret, S., Isabel Pividori, M., 2010. A novel strategy for screening-out raw milk contaminated with Mycobacterium bovis on dairy farms by double-tagging PCR and electrochemical genosensing. Int. Microbiol. 13, 91–97. https://doi.org/10.2436/20.1501.01.114.

Logan, N., Lou Franco, J., Elliott, C., Cao, C., 2021. Catalytic gold nanostars for SERS-based detection of mercury ions (Hg2+) with inverse sensitivity. Environ. Sci. Nano 8, 2718–2730. https://doi.org/10.1039/d1en00548k.

Lombardi, G., Botti, I., Pacciarini, M.L., Boniotti, M.B., Roncarati, G., Dal Monte, P., 2017. Five-year surveillance of human tuberculosis caused by Mycobacterium bovis in Bologna, Italy: an underestimated problem. Epidemiol. Infect. 145, 3035–3039. https://doi.org/10.1017/S0950268817001996.

Lou-Franco, J., Das, B., Elliott, C., Cao, C., 2021. Gold nanozymes: from concept to biomedical applications. Nano-Micro Lett. 13, 1–36. https://doi.org/10.1007/s40820-020-00532-z.

Lou, D., Tian, Y., Zhang, Y., Yin, J., Yang, T., He, C., Ma, M., Yu, W., Gu, N., 2018. Peroxidase-like activity of gold nanoparticles and their gold staining enhanced ELISA application. J. Nanosci. Nanotechnol. 18, 951–958. https://doi.org/10.1166/jnn.2018.13977.

Love, J.C., Estroff, L.A., Kriebel, J.K., Nuzzo, R.G., Whitesides, G.M., 2005. Self-assembled monolayers of thiolates on metals as a form of nanotechnology. Chem. Rev. 105, 1103–1169. https://doi.org/10.1021/cr0300789.

Lozano, R., Naghavi, M., Foreman, K., Lim, S., Shibuya, K., Aboyans, V., Abraham, J., Adair, T., Aggarwal, R., Ahn, S.Y., AlMazroa, M.A., Alvarado, M., Anderson, H.R., Anderson, L.M., Andrews, K.G., Atkinson, C., Baddour, L.M., Barker-Collo, S., Bartels, D.H., Bell, M.L., Benjamin, E.J., Bennett, D., Bhalla, K., Bikbov, B., Bin Abdulhak, A., Birbeck, G., Blyth, F., Bolliger, I., Boufous, S., Bucello, C., Burch, M., Burney, P., Carapetis, J., Chen, H., Chou, D., Chugh, S.S., Coffeng, L.E., Colan, S.D., Colquhoun, S., Colson, K.E., Condon, J., Connor, M.D., Cooper, L.T., Corriere, M.,

Cortinovis, M., Courville De Vaccaro, K., Couser, W., Cowie, B.C., Criqui, M.H., Cross, M., Dabhadkar, K.C., Dahodwala, N., De Leo, D., Degenhardt, L., Delossantos, A., Denenberg, J., Des Jarlais, D.C., Dharmaratne, S.D., Dorsey, E.R., Driscoll, T., Duber, H., Ebel, B., Erwin, P.J., Espindola, P., Ezzati, M., Feigin, V., Flaxman, A.D., Forouzanfar, M.H., Fowkes, F.G.R., Franklin, R., Fransen, M., Freeman, M.K., Gabriel, S.E., Gakidou, E., Gaspari, F., Gillum, R.F., Gonzalez-Medina, D., Halasa, Y.A., Haring, D., Harrison, J.E., Havmoeller, R., Hay, R.J., Hoen, B., Hotez, P.J., Hoy, D., Jacobsen, K.H., James, S.L., Jasrasaria, R., Jayaraman, S., Johns, N., Karthikeyan, G., Kassebaum, N., Keren, A., Khoo, J.P., Knowlton, L.M., Kobusingye, O., Koranteng, A., Krishnamurthi, R., Lipnick, M., Lipshultz, S.E., Lockett Ohno, S., Mabweijano, J., MacIntyre, M.F., Mallinger, L., March, L., Marks, G.B., Marks, R., Matsumori, A., Matzopoulos, R., Mayosi, B.M., McAnulty, J.H., McDermott, M.M., McGrath, J., Memish, Z.A., Mensah, G.A., Merriman, T.R., Michaud, C., Miller, M., Miller, T.R., Mock, C., Mocumbi, A.O., Mokdad, A.A., Moran, A., Mulholland, K., Nair, M.N., Naldi, L., Narayan, K.M.V., Nasseri, K., Norman, P., O'Donnell, M., Omer, S.B., Ortblad, K., Osborne, R., Ozgediz, D., Pahari, B., Pandian, J.D., Panozo Rivero, A., Perez Padilla, R., Perez-Ruiz, F., Perico, N., Phillips, D., Pierce, K., Pope, C.A., Porrini, E., Pourmalek, F., Raju, M., Ranganathan, D., Rehm, J.T., Rein, D.B., Remuzzi, G., Rivara, F.P., Roberts, T., Rodriguez De León, F., Rosenfeld, L.C., Rushton, L., Sacco, R.L., Salomon, J.A., Sampson, U., Sanman, E., Schwebel, D.C., Segui-Gomez, M., Shepard, D.S., Singh, D., Singleton, J., Sliwa, K., Smith, E., Steer, A., Taylor, J.A., Thomas, B., Tleyjeh, I.M., Towbin, J.A., Truelsen, T., Undurraga, E.A., Venketasubramanian, N., Vijayakumar, L., Vos, T., Wagner, G.R., Wang, M., Wang, W., Watt, K., Weinstock, M.A., Weintraub, R., Wilkinson, J.D., Woolf, A.D., Wulf, S., Yeh, P.H., Yip, P., Zabetian, A., Zheng, Z.J., Lopez, A.D., Murray, C.J.L., 2012. Global and regional mortality from 235 causes of death for 20 age groups in 1990 and 2010: a systematic analysis for the Global Burden of Disease Study 2010. Lancet 380, 2095–2128. https://doi.org/10.1016/S0140-6736(12)61728-0.

Ma, T., Yang, W., Liu, S., Zhang, H., Liang, F., 2017. A comparison reduction of 4-nitrophenol by gold nanospheres and gold nanostars. Catalysts 7, 1–10. https://doi.org/10.3390/catal7020038.

Matos, A.C., Figueira, L., Martins, M.H., Pinto, M.L., Matos, M., Coelho, A.C., 2016. New insights into Mycobacterium bovis prevalence in wild mammals in Portugal. Transbound. Emerg. Dis. 63, 313–322. https://doi.org/10.1111/tbed.12306.

McVey, C., Logan, N., Thanh, N.T.K., Elliott, C., Cao, C., 2019. Unusual switchable peroxidase-mimicking nanozyme for the determination of proteolytic biomarker. Nano Res. 12, 509–516. https://doi.org/10.1007/s12274-018-2241-3.

Murphy, C.J., Sau, T.K., Gole, A.M., Orendorff, C.J., Gao, J., Gou, L., Hunyadi, S.E., Li, T., 2005. Anisotropic metal nanoparticles: synthesis, assembly, and optical applications. J. Phys. Chem. B 109, 13857–13870. https://doi.org/10.1021/jp0516846.

Nelis, J.L.D., Bura, L., Zhao, Y., Burkin, K.M., Rafferty, K., Elliott, C.T., Campbell, K., 2019a. The efficiency of color space channels to quantify color and color intensity change in liquids, pH strips, and lateral flow assays with smartphones. Sensors 19, 5104. https://doi.org/10.3390/s19235104.

Nelis, J.L.D., Tsagkaris, A.S., Zhao, Y., Lou-Franco, J., Nolan, P., Zhou, H., Cao, C., Rafferty, K., Hajslova, J., Elliott, C.T., Campbell, K., 2019b. The end user sensor tree: an end-user friendly sensor database. Biosens. Bioelectron. 130, 245–253. https://doi.org/10.1016/j.bios.2019.01.055.

Nelis, J.L.D., Zhao, Y., Zhao, Y., Bura, L., Rafferty, K., Elliott, C.T., Campbell, K., 2020. A randomized combined channel approach for the quantification of color- and intensity-based assays with smartphones. Anal. Chem. 92, 7852–7860. https://doi.org/10.1021/acs.analchem.0c01099.

Pai, S.S., Hammouda, B., Hong, K., Pozzo, D.C., Przybycien, T.M., Tilton, R.D., 2011. The conformation of the poly(ethylene glycol) chain in mono-PEGylated lysozyme and mono-PEGylated human growth hormone. Bioconjugate Chem. 22, 2317–2323. https://doi.org/10.1021/bc2003583.

Pathak, S., Davidson, M.C., Silva, G.A., 2007. Characterization of the functional binding properties of antibody conjugated quantum dots. Nano Lett. 7, 1839–1845. https://doi.org/10.1021/nl062706i.

Pawar, S., Bhattacharya, A., Nag, A., 2019. Metal-enhanced fluorescence study in aqueous medium by coupling gold nanoparticles and fluorophores using a bilayer vesicle platform. ACS Omega 4, 5983–5990. https://doi.org/10.1021/acsomega.9b00036.

Rodríguez-Lorenzo, L., De La Rica, R., Álvarez-Puebla, R.A., Liz-Marzán, L.M., Stevens, M.M., 2012. Plasmonic nanosensors with inverse sensitivity by means of enzyme-guided crystal growth. Nat. Mater. 11, 604–607. https://doi.org/10.1038/nmat3337.

Sajanlal, P.R., Sreeprasad, T.S., Samal, A.K., Pradeep, T., 2011. Anisotropic nanomaterials: structure, growth, assembly, and functions. Nano Rev. 2, 5883. https://doi.org/10.3402/nano.v2i0.5883.

Serrano-Montes, A.B., Langer, J., Henriksen-Lacey, M., Jimenez De Aberasturi, D., Solís, D.M., Taboada, J.M., Obelleiro, F., Sentosun, K., Bals, S., Bekdemir, A., Stellacci, F., Liz-Marzán, L.M., 2016. Gold nanostar-coated polystyrene beads as multifunctional nanoprobes for SERS bioimaging. J. Phys. Chem. C 120, 20860–20868. https://doi.org/10.1021/acs.jpcc.6b02282.

Silva, L.B., Veigas, B., Doria, G., Costa, P., Inácio, J., Martins, R., Fortunato, E., Baptista, P.V., 2011. Portable optoelectronic biosensing platform for identification of mycobacteria from the Mycobacterium tuberculosis complex. Biosens. Bioelectron. 26, 2012–2017. https://doi.org/10.1016/j.bios.2010.08.078.

Stewart, L.D., McNair, J., McCallan, L., Thompson, S., Kulakov, L.A., Grant, I.R., 2012. Production and evaluation of antibodies and phage display-derived peptide ligands for immunomagnetic separation of Mycobacterium bovis. J. Clin. Microbiol. 50, 1598–1605. https://doi.org/10.1128/JCM.05747-11.

Stewart, L.D., Tort, N., Meakin, P., Argudo, J.M., Nzuma, R., Reid, N., Delahay, R.J., Ashford, R., Montgomery, W.I., Grant, I.R., 2017. Development of a novel immunochromatographic lateral flow assay specific for Mycobacterium bovis cells and its application in combination with immunomagnetic separation to test badger faeces. BMC Vet. Res. 13, 1–12. https://doi.org/10.1186/s12917-017-1048-x.

Thoen, C.O., Steele, J.H., Kaneene, J.B. (Eds.), 2014. Zoonotic Tuberculosis. Mycobacterium Bovis and Other Pathogenic Mycobacteria, third ed. ed. Wiley Blackwell.

Torres-Gonzalez, P., Cervera-Hernandez, M.E., Martinez-Gamboa, A., Garcia-Garcia, L., Cruz-Hervert, L.P., Bobadilla-del Valle, M., Ponce-de Leon, A., Sifuentes-Osornio, J., 2016. Human tuberculosis caused by Mycobacterium bovis: a retrospective comparison with Mycobacterium tuberculosis in a Mexican tertiary care centre, 2000-2015. BMC Infect. Dis. 16, 1–9. https://doi.org/10.1186/s12879-016-2001-5.

Wang, R.L.C., Kreuzer, H.J., Grunze, M., 1997. Molecular conformation and solvation of oligo(ethylene glycol)-terminated self-assembled monolayers and their resistance to protein adsorption. J. Phys. Chem. B 101, 9767–9773. https://doi.org/10.1021/jp9716952.

World Health Organization, 2019. Global tuberculosis report-executive summary. World Health Organization, pp. 1–8.

Zayats, M., Baron, R., Popov, I., Willner, I., 2005. Biocatalytic growth of Au nanoparticles: from mechanistic aspects to biosensors design. Nano Lett. 5, 21–25. https://doi.org/10.1021/nl048547p.

Zhao, Y., Choi, S.Y., Lou-Franco, J., Nelis, J.L.D., Zhou, H., Cao, C., Campbell, K., Elliott, C., Rafferty, K., 2019. Smartphone modulated colorimetric reader with color subtraction. In: IEEE Sensors. Accept. Publ, pp. 1–4. https://doi.org/10.1109/SENSORS43011.2019.8956565, 2019.

Zhao, Y., Elliott, C., Zhou, H., Rafferty, K., 2018. Spectral illumination correction: achieving relative color constancy under the spectral domain. In: IEEE International Symposium on Signal Processing and Information Technology (ISSPIT). IEEE, pp. 690–695. https://doi.org/10.1109/ISSPIT.2018.8642637, 2018.